ICSV14
Cairns • Australia
9-12 July, 2007

14th International Congress on Sound & Vibration

ACOUSTIC WAVE PROPAGATION MODELING FOR PERIODIC STRUCTURES AS APPLIED TO ANECHOIC COATING DESIGN

Sven Ivansson[1]

[1]Department of Underwater Research, Swedish Defence Research Agency
Stockholm, SE-16490, Sweden
sveni@foi.se (email address of lead author or presenter)

Abstract

A thin rubber coating with cavities in a doubly periodic lattice can redistribute sound energy, normally incident on a steel plate, in the lateral direction. An anechoic effect appears by absorption in the surrounding rubber. This effect is modeled and studied by adapting modern semianalytical computation techniques for electron scattering and band gaps in connection with photonic and phononic crystals. In comparison to more flexible but also more computer intensive methods, such as FEM modeling, there are two advantages. First, an improved physical understanding of the anechoic effect can be achieved by simplified semianalytical analysis. The viscoelastic shear-wave properties of the rubber are crucial for generating the desired loss, but compressional-wave absorption can be useful to reduce the reflectance at higher frequencies. The second advantage is the computational speed, which allows modern global optimization techniques to be applied for coating design. Differential evolution algorithms are used to design coatings with significant echo reduction within broad frequency intervals. Computational speed is enhanced by utilizing symmetry properties to reduce the size of the pertinent equation systems. The fastest computations are obtained for spherical cavities of a common size, but extensions to mixed cavity sizes are shown to be possible and useful.

1. INTRODUCTION

Rubber coatings with air-filled cavities or scatterers can be used on submarines for anechoic purposes [1]. Such coatings are said to be of Alberich type. When sound from an active sonar enters the coating, Fig. 1, energy that is scattered by the cavities can be absorbed by the rubber material, and the reflection amplitude can be reduced significantly.

Reflections of normally incident plane waves by steel plates with Alberich coatings have been modeled numerically in [2]-[4] with a semi-analytical method borrowed from atomic physics [5] and applied in recent years to studies of band gaps for photonic and phononic crystals [6],[7]. Sound propagation through a sequence of layers, with or without cavities, is handled recursively by the invariant embedding or Riccati method [8]. The wave field scattered by each cavity is expanded in spherical wave functions, and multiple scattering among the cavities is incorporated in a rigorous self-consistent way. Transformation formulas between spherical and plane waves provide the coupling to the plane waves needed for the recursive invariant embedding treatment of multi-layered cases. The mechanism of the echo reduction was studied in [2] and [3]. Cavities filled with soft or hard material can be used, with monopole and dipole scattering, respectively, as important mechanisms. Effects of multiple scattering among the cavities are seen to be noticeable in both cases. With hard inclusions, the multiple scattering is even crucial and a dense grid is required. Experimental results to verify high-frequency scattering in nonnormal directions were included in [4]. Coating design by global optimization was attempted in [3] and [4].

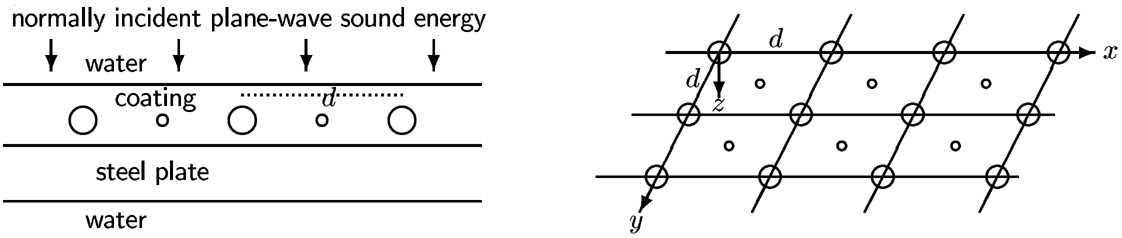

Figure 1. *Left*: A steel plate in water is covered with an Alberich rubber coating with spherical cavities of two sizes. *Right*: The cavity lattice with period *d* is viewed from another perspective. Horizontal *xy* coordinates are introduced along with a *z* coordinate axis. The rotation angle between the *xy* axes and the lattice period directions, denoted χ in the text, vanishes in this illustration.

For each cavity interface, the cavities in [2]-[4] were assumed to be identical and spherical. After a brief review of the basic computational method, it is described in the present paper how cavities of different sizes can be included in the same cavity interface, and symmetry properties are utilized to enhance computational speed. Applications to coating design and loss distribution computations are presented.

2. BASIC COMPUTATIONAL METHOD

As in Fig. 1, a right-hand Cartesian *xyz* coordinate system is introduced in a fluid-solid medium surrounded by homogeneous half-spaces. The medium is periodic with period *d* in horizontal directions rotated an angle χ from the *x* and *y* directions, respectively. Sound waves with time dependence $\exp(-i\omega t)$, to be suppressed in the formulas, are considered, where ω is the angular frequency. It follows that an incident plane wave with horizontal wavenumber vector $\mathbf{k}_{\|}$ will give rise to a linear combination of reflected and transmitted plane waves with displacement vectors

$$\mathbf{u}(\mathbf{r}) = \exp(\mathrm{i}\, \mathbf{K}_{\mathbf{g}j}{}^{s}\cdot\mathbf{r})\cdot\mathbf{e}_j \,. \tag{1}$$

Here, $\mathbf{r}=(x,y,z)$, j=1,2,3 for a wave of type P,SV,SH, respectively, s=+(−) for a wave in the positive (negative) z direction, and

$$\mathbf{K}_{\mathbf{g}j}{}^{\pm} = \mathbf{k}_{\|} + \mathbf{g} \pm [\, (\omega/c_j)^2 - |\mathbf{k}_{\|} + \mathbf{g}|^2 \,]^{1/2}\cdot(0,0,1) = \omega/c_j\cdot(\sin\theta \cos\varphi,\, \sin\theta \sin\varphi,\, \cos\theta) \tag{2}$$

where **g** belongs to the reciprocal lattice

$$\mathbf{g} = (k_x,k_y,0) = 2\pi m/d\cdot(\cos\chi,\, \sin\chi,\, 0) + 2\pi n/d\cdot(-\sin\chi,\, \cos\chi,\, 0) \tag{3}$$

where m and n are integers. Furthermore, c_j is the compressional-wave velocity α when j=1 and the shear-wave velocity β when j=2,3. The angular variables θ,φ of $\mathbf{K}_{\mathbf{g}j}^{\pm}$ are defined by (2), with a possibly complex cos θ. The vectors $\mathbf{e}_j = \mathbf{e}_j(\mathbf{K}_{\mathbf{g}j}^{\pm})$, are defined by $\mathbf{e}_1 = (\sin\theta\cos\varphi, \sin\theta\sin\varphi, \cos\theta)$, $\mathbf{e}_2 = (\cos\theta\cos\varphi, \cos\theta\sin\varphi, -\sin\theta)$, $\mathbf{e}_3 = (-\sin\varphi, \cos\varphi, 0)$.

As detailed in [2]-[4], and references therein, reflection and transmission matrices R_B,T_B and R_A,T_A can now be introduced, for the discrete set of waves specified by (1)-(3). Including one scatterer interface within the rubber layer, four interfaces are involved in the left panel of Fig. 1. Individual R/T matrices can be combined recursively [5],[8], and layer thicknesses are conveniently accounted for by phase shifts.

2.1 Interface with Periodically Distributed Scatterers of a Common Type

Explicit expressions for the R/T matrices are well known for an interface between two homogeneous half-spaces [8]. Spherical vector solutions to the wave equations can be used to handle an interface with periodically distributed scatterers [6]. As in [2]-[4], $\mathbf{u}_{lm}^{0L}(\mathbf{r})$, $\mathbf{u}_{lm}^{0M}(\mathbf{r})$, $\mathbf{u}_{lm}^{0N}(\mathbf{r})$ and $\mathbf{u}_{lm}^{+L}(\mathbf{r})$, $\mathbf{u}_{lm}^{+M}(\mathbf{r})$, $\mathbf{u}_{lm}^{+N}(\mathbf{r})$ are here used to denote regular solutions involving the spherical Bessel function j_l and outgoing solutions involving the spherical Hankel function h_l^+, respectively. The L and N solutions are spheroidal, while the M solutions are toroidal. The pertinent wave velocity is α for the L solutions, and β for the M and N solutions. The index l=0,1,2,.. with m=−l,..,l, since the spherical harmonics are involved, but it is understood that $\mathbf{u}_{00}^{0M} \equiv \mathbf{u}_{00}^{0N} \equiv \mathbf{u}_{00}^{+M} \equiv \mathbf{u}_{00}^{+N} \equiv \mathbf{0}$. For scatterers at $\mathbf{R} = md\cdot(\cos\chi, \sin\chi, 0) + nd\cdot(-\sin\chi, \cos\chi, 0)$, with integers m,n, and an incident plane wave as in (1), the total scattered field $\mathbf{u}_{sc}$ can be written [6]

$$\mathbf{u}_{sc}(\mathbf{r}) = \textstyle\sum_{Plm} [\, b_{lm}^{+P} \sum_{\mathbf{R}} \exp(i\, \mathbf{k}_{\|}\cdot\mathbf{R})\cdot\mathbf{u}_{lm}^{+P}(\mathbf{r}-\mathbf{R}) \,], \qquad P = L,M,N. \tag{4}$$

The vector $\mathbf{b}^+ = \{b_{lm}^{+P}\}$ is determined by solving the equation system

$$(\, \mathbf{I} - T\cdot\Omega \,)\cdot\mathbf{b}^+ = T\cdot\mathbf{a}^0 \tag{5}$$

where $\mathbf{I}$ is the appropriate identity matrix, $\mathbf{a}^0 = \{a_{lm}^{0P}\}$ gives the coefficients for expansion of the incident plane wave in regular spherical waves $\mathbf{u}_{lm}^{0P}(\mathbf{r})$, $\Omega = \Omega(d, \chi, \mathbf{k}_{\|}, \omega/\alpha, \omega/\beta)$ is the lattice translation matrix $\{\Omega_{lm;l'm'}^{PP'}\}$, and $T = \{T_{lm;l'm'}^{PP'}\}$ is the transition matrix for an individual scatterer. Specifically, $\mathbf{b}' = \Omega\cdot\mathbf{b}^+$ and $\mathbf{b}^+ = T\cdot(\mathbf{a}^0+\mathbf{b}')$ where $\mathbf{b}' = \{b_{lm}^{'P}\}$ gives the coefficients for expansion in regular spherical waves $\mathbf{u}_{lm}^{0P}$ of the scattered field from all scatterers except the one at the origin. A computer program for calculating Ω can be found in [5].

The R/T matrices are obtained, finally, by transforming the expansion (4) to plane waves of the type (1).

3. EXTENSIONS

3.1 Different Types of Scatterers in the Same Plane

As illustrated in Fig. 1, a particular case with two types of scatterers in the xy plane is considered here. Scatterers of the first type, with transition matrix T and scattered-field expansion coefficients denoted $\mathbf{b}^+$, appear at $\mathbf{R} = m\cdot(d,0,0) + n\cdot(0,d,0)$, for integers m,n. Scatterers of the second type, with transition matrix U and scattered-field expansion coefficients denoted $\mathbf{c}^+$, appear at points $\mathbf{S}$ in between, i.e., $\mathbf{S} = (m+½)\cdot(d,0,0) + (n+½)\cdot(0,d,0)$. The reciprocal lattice vectors become $\mathbf{g} = (2\pi m/d, 2\pi n/d, 0)$, where m,n run over the integers.

The generalization of the expression (4) for the scattered field becomes

$$\mathbf{u}_{\mathrm{sc}}(\mathbf{r}) = \sum_{Plm} [\, b_{lm}^{+P} \sum_{\mathbf{R}} \exp(\mathrm{i}\, \mathbf{k}_{\|}\cdot\mathbf{R})\cdot\mathbf{u}_{lm}^{+P}(\mathbf{r}-\mathbf{R})\,] + \sum_{Plm} [\, c_{lm}^{+P} \sum_{\mathbf{S}} \exp(\mathrm{i}\, \mathbf{k}_{\|}\cdot\mathbf{S})\cdot\mathbf{u}_{lm}^{+P}(\mathbf{r}-\mathbf{S})\,] \,. \tag{6}$$

It follows that

$$\mathbf{b}^{+} = T \cdot (\mathbf{a}^{0}+\mathbf{b}'+\mathbf{b}'') \qquad \text{and} \qquad \mathbf{c}^{+} = U \cdot (\mathbf{a}^{0}+\mathbf{c}'+\mathbf{c}'') \tag{7}$$

where, for a scatterer of the first type at the origin, **b**' and **b**" give the coefficients for expansion in regular spherical waves of the scattered field from all other scatterers of the same and the different type, respectively. The vectors **c**' and **c**" are defined analogously for a scatterer of the second type, in a translated coordinate system with this scatterer at the origin and a phase shifted incident plane wave to get phase zero at the new origin.

With $\Omega^0 = \Omega(d, 0, \mathbf{k}_{\|}, \omega/\alpha, \omega/\beta)$, it follows that $\mathbf{b}' = \Omega^0 \cdot \mathbf{b}^+$ and $\mathbf{c}' = \Omega^0 \cdot \mathbf{c}^+$. For a certain matrix Q, to be determined, $\mathbf{b}'' = \mathrm{Q} \cdot \mathbf{c}^+$ and $\mathbf{c}'' = \mathrm{Q} \cdot \mathbf{b}^+$. The equation system for determination of $\mathbf{b}^+$ and $\mathbf{c}^+$ becomes

$$\begin{aligned} (\, \mathbf{I} - T\cdot \Omega^0\,) \cdot \mathbf{b}^+ - T\cdot \mathrm{Q} \cdot \mathbf{c}^+ &= T \cdot \mathbf{a}^0. \\ - U\cdot \mathrm{Q} \cdot \mathbf{b}^+ + (\, \mathbf{I} - U\cdot \Omega^0\,) \cdot \mathbf{c}^+ &= U \cdot \mathbf{a}^0. \end{aligned} \tag{8}$$

In order to form the R/T matrices, incident plane waves with different horizontal wavenumber vectors $\mathbf{k}_{\|}+\mathbf{g}_{\mathrm{inc}}$ have to be considered, where $\mathbf{g}_{\mathrm{inc}}$ belongs to the reciprocal lattice $\{(2\pi m/d,\ 2\pi n/d,\ 0)\}$. Noting that the union of the scatterer positions is a small square lattice with period $d/\sqrt{2}$ tilted an angle $\pi/4$ with respect to the xy axes, the following expression for Q as a difference of Ω matrices is directly obtained

$$\mathrm{Q} = \Omega(d/\sqrt{2}, \pi/4, \mathbf{k}_{\|}+\mathbf{g}_{\mathrm{inc}}, \omega/\alpha, \omega/\beta) - \Omega^0 \,. \tag{9}$$

Only those $\mathbf{g}_{\mathrm{inc}}$ in $\{(2\pi m/d,\ 2\pi n/d,\ 0)\}$ for which $m-n$ is even are reciprocal vectors for the small tilted lattice. Since a lattice translation matrix Ω is periodic in its third argument with the same periods as the corresponding reciprocal lattice, there will be two groups of $\mathbf{g}_{\mathrm{inc}}$ with different Q matrices according to (9).

The transformation of the expansion (6) to plane waves of the type (1) can be done separately for each of the **R** and **S** sums. In the latter case, the translation from the origin causes a sign change for some combinations of incident ($\mathbf{g}_{\mathrm{inc}}$) and scattered ($\mathbf{g}_{\mathrm{sc}}$) reciprocal lattice vectors.

In this development, the two types of scatterers appear in the same horizontal plane with the **S** points midway between the **R** points. By applying translation formulas for spherical wave functions, e.g., [5] (Sec. IVC), it should be possible to treat more general cases.

3.2 Equation System Split

For the case of a spherical scatterer, explicit analytical expressions can be given for the transition matrix $T = \{T_{lm;l'm'}^{PP'}\}$, e.g., [6]. Furthermore, scattering only appears to the same l,m components ($l'=l$, $m'=m$), and also to the same type ($P'=P$) except that L waves can be scattered to N waves and vice versa. The matrices Ω have the following properties [6],[9]

- compressional- and shear-wave elements are not mixed, i.e., $\Omega_{lm;l'm'}^{PP'}$ vanishes when precisely one of P,P', is L and the other one is M or N
- $\Omega_{lm;l'm'}^{LL}$, $\Omega_{lm;l'm'}^{MM}$ and $\Omega_{lm;l'm'}^{NN}$ vanish unless $(l'+m')-(l+m)$ is even
- $\Omega_{lm;l'm'}^{MN}$ and $\Omega_{lm;l'm'}^{NM} = -\Omega_{lm;l'm'}^{MN}$ vanish unless $(l'+m')-(l+m)$ is odd.

As is well known, e.g., [5], it follows by considering $T\cdot\,\Omega$ that the equation system (5) can be split into two subsystems. One subsystem concerns the b_{lm}^{+L}, b_{lm}^{+N} with odd l+m together with the b_{lm}^{+M} with even l+m , while the other subsystem concerns the b_{lm}^{+L}, b_{lm}^{+N} with even l+m together with the b_{lm}^{+M} with odd l+m.

It is easily realized that the equation system (8) can be split into two subsystems by combining $\mathbf{b}^{+}$- and $\mathbf{c}^{+}$-vector elements in an analogous way.

3.3 Utilizing Symmetry

The recursive combination of individual R/T matrices [5],[8] involves matrix inversions, where the matrix dimension equals the finite number of plane waves according to (1)-(3), which are chosen to be included. For a compressional wave at normal incidence, $\mathbf{k}_{||}$=$\mathbf{0}$, on the square scatterer lattice(s), symmetry arguments directly show that many of the reflected and transmitted plane waves will have equal coefficients. By forming a new wave basis from sums of plane waves with equal scattering coefficients, a matrix dimension reduction is achieved with almost a factor of eight. The waves with horizontal wavenumber vectors in the x, y, and diagonal directions must be combined in groups of four waves, rather than eight, and normally incident waves must be taken separately. The dramatic reduction of computation time that results is essential for the coating design examples to be considered in Sec. 4.

Each sum of plane waves is expanded in regular spherical waves to get the $\mathbf{a}^0$ vectors for the equation systems (5) and (8). As pointed out in [5] (Sec. IVH), symmetry arguments make it possible to reduce the dimensions of these equation systems as well.

4. COATING DESIGN

Global optimization methods can be used to design anechoic coatings. Simulated annealing, genetic algorithms, and differential evolution (DE) are three kinds of such methods, that have become popular during the last fifteen years. DE, to be applied here, is related to genetic algorithms, but the parameters are not encoded in bit strings, and genetic operators such as crossover and mutation are replaced by algebraic operators. For applications to underwater acoustics, DE has been claimed to be much more efficient than genetic algorithms [10] and comparable in efficiency to a modern adaptive simplex simulated annealing algorithm [11].

Fig. 2 shows four cases, I_0,II_0,I_a,II_a, of optimized coatings with air-filled spherical cavities as illustrated in Fig. 1. The steel plate is 4 mm thick, and it is immersed in water with sound velocity c = 1480 m/s. The steel parameters are 5850 and 3230 m/s for the compressional- and shear-wave velocities, respectively, and 7.7 kg/dm^3 for the density. Only the rubber, modelled as a viscoelastic solid, is anelastic.

The objective function for DE minimization was specified as the maximum reflectance, i.e., time- (and space-) averaged reflected energy flux relative to the time-averaged energy flux of a normally incident monofrequency plane compressional wave, in the frequency band 15-30 kHz. For case II_a, right panel in Fig. 2, ten parameters, denoted p_1,p_2,..,p_{10}, were varied within the following search space: rubber density [p_1, 0.9-1.3 kg/dm^3], rubber compressional-wave velocity [p_2, 1450-1550 m/s] and absorption [p_3, 0-25 dB/wavelength], rubber shear-wave velocity [p_4, 70-150 m/s] and absorption [p_5, 7-27 dB/wavelength], and lattice period [p_6=d, 7-20 mm], coating thickness [p_7, 2-5 mm], largest cavity diameter [0.5mm+$p_8\cdot$(p_7-2mm)] and cavity diameter quotient [p_9, 0.5-1], outer coating thickness between water and largest cavities [1.5mm+ $p_{10}\cdot$(p_7-2mm)]. The parameters p_8 and p_{10} were defined as fractions such that p_8+$p_{10} \leq 1$.

Cases I differ from cases II by exclusion of the smallest cavities (p_9=0). Cases I_0 and II_0, left panel of Fig. 2, differ from cases I_a and II_a, right panel, by omission (essentially) of the compressional-wave absorption (p_3=0.1 dB/wavelength).

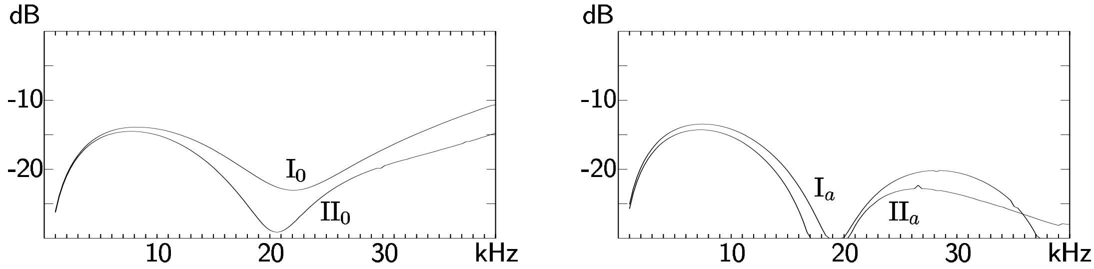

Figure 2. Reflectancies in dB as functions of frequency for four DE optimization cases described in the text: I_0,II_0 to the left and I_a,II_a to the right. Some 40000 coating models were tested during the optimization for each case.

Table 1 shows the optima along with corresponding parameter values. An echo reduction of almost 23 dB is achieved throughout the band 15-30 kHz with a coating of type II_a. Comparing cases I and II, inclusion of mixed cavity sizes brings about an improvement of 2.6 dB in these examples. Half the optimum lattice periods *d* for the two cases II are 8.3 and 9.95 mm, respectively, and it should be noted that the search region for parameter $p_6=d$ (7-20 mm) allows coatings with equally densely spaced but equal cavities for the two cases I. The compressional-wave absorption is useful to improve the high-frequency performance.

Thick, light, and soft coatings (large p_7, small p_1, and small p_2) with high shear-wave absorption (large p_5) and large cavities (large p_8 and p_7) are typically preferred. As illustrated in [4] for a case similar to case I_0 here but allowing smaller outer coating thickness, identification of the parts of the parameter space resulting in favorable anechoic properties can be aided by a stochastic resampling algorithm borrowed from inverse theory [12].

Table 1. Optima found by DE, with corresponding values of varied parameters.

	Case I_0	**Case II_0**	**Case I_a**	**Case II_a**
optimum	-17.2 dB	-19.8 dB	-20.2 dB	-22.8 dB
p_1	0.900 kg/dm^3	0.900 kg/dm^3	0.900 kg/dm^3	0.901 kg/dm^3
p_2	1453 m/s	1457 m/s	1450 m/s	1450 m/s
p_3			20.9 dB	13.2 dB
p_4	149 m/s	135 m/s	145 m/s	123 m/s
p_5	26.9 dB	26.8 dB	26.7 dB	25.3 dB
$p_6=d$	13.7 mm	16.6 mm	19.1 mm	19.9 mm
p_7	4.997 mm	4.949 mm	4.999 mm	4.980 mm
p_8	0.925	0.975	0.991	0.940
p_9		0.570		0.565
p_{10}	0.008	0.008	0.006	0.002

Further results concerning cases II_0 and II_a are presented in the left panels of Figs. 3 and 4, respectively. It is shown how the energy flux of the normally incident plane wave is divided into reflected flux, transmitted flux, and absorption in the rubber. The panels to the right illustrate the significance of the cavities by showing corresponding results for corresponding rubber coatings without cavities.

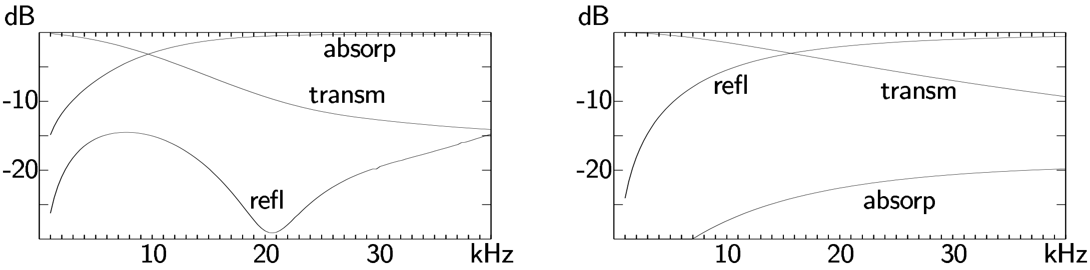

Figure 3. *Left*: The reflectance curve for case II_0 is copied from the left panel of Fig. 2 and shown together with the corresponding transmittance and absorption loss curves. *Right*: Corresponding results are shown for a similar coating without cavities.

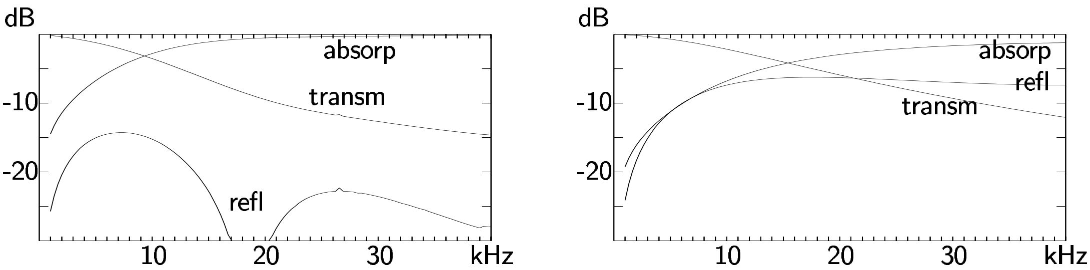

Figure 4. *Left*: The reflectance curve for case II_a is copied from the right panel of Fig. 2 and shown together with the corresponding transmittance and absorption loss curves. *Right*: Corresponding results are shown for a similar coating without cavities.

5. ABSORPTION LOSS DISTRIBUTION

As explained in [2], the plane waves approaching the cavity lattice(s) from above and below can be determined, and the wave field around a cavity can subsequently be expanded in spherical waves. It follows that the absorption in a spherical rubber shell around each cavity can easily be computed. Examples for the two cases II are given in Fig. 5, with the largest possible spherical shell to fit into the rubber layer in each case. The outer shell radius is thus 1.739 mm in case II_0 and 1.823 mm in case II_a.

The cavity radii in case II_0 are 1.687 mm and 0.962 mm, and the corresponding shells occupy only 0.14 % and 1.34 % of the rubber volume, respectively. In case II_a, the corresponding shell volume fractions are 0.33 % and 1.11 %, for cavity radii 1.650 mm and 0.932 mm, respectively. Hence, by the (b) and (c) curves of Fig. 5, a disproportionately large part of the absorption loss takes place in the specified shells, in comparison to their volumes.

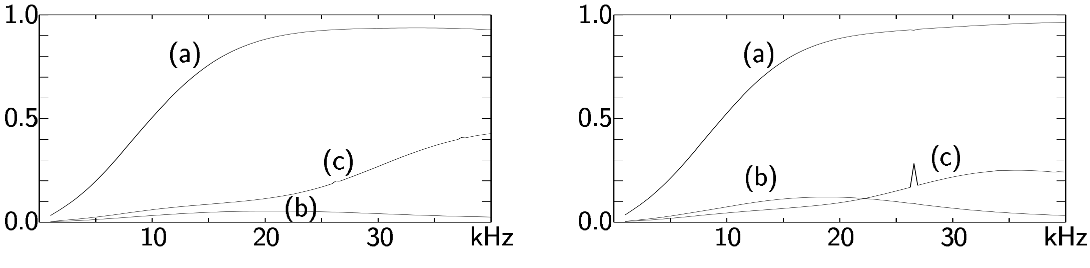

Figure 5. The left and right panels concern cases II_0 and II_a, respectively. In each case, curve (a) shows the fraction of the incident energy flux that is absorbed. Transformed to dB, these curves have already appeared in Figs. 3 and 4. The (b) and (c) curves show the fraction of the incident energy flux

that is absorbed in certain cavity-enclosing spherical shells specified in the text. In each case, the (b) results are for the largest cavities and the (c) results are for the smallest ones.

6. CONCLUSIONS

A fast semi-analytical technique for computing scattering from layers including doubly periodic scatterer lattices has been extended to cases with spherical cavities of two different sizes in the same horizontal plane. Applications to design of anechoic coatings with a differential evolution algorithm for global optimization indicate improvements by almost three dB of the reflection reduction that can be achieved. The small cavities in the suggested coatings have radii of about 57 % of the radii of the large cavities. Symmetry arguments are used to reduce equation system dimensions and enhance speed in the repeated computations.

Rubber compressional-wave absorption can be useful to enhance the echo reduction in the high-frequency regime. The cavities and the shear-wave absorption in the rubber are essential, however, to produce a good performance with a reasonably thin coating. The absorption loss that takes place in the vicinity of the cavities is disproportionately large, as shown by explicit computations.

Work is in progress concerning extensions to nonspherical cavities, for which transmission matrices can be computed numerically, e.g., [13]. Further improvements are expected concerning the coatings that can be designed.

REFERENCES

[1] H. Oberst "Resonant sound absorbers", in E.G. Richardson (ed.) *Technical aspects of sound*, 1957, pp. 421-439.

[2] S. Ivansson "Sound absorption by viscoelastic coatings with periodically distributed cavities", *J. Acoust. Soc. Am.* **119**, 3558-3567 (2006).

[3] S. Ivansson "Numerical modelling for design of viscoelastic coatings with favorable sound absorbing properties", *Nonlin. Anal.* **63**, e1541-e1550 (2005).

[4] S. Ivansson "Reflections from steel plates with doubly periodic anechoic coatings", in A. Tolstoy, E.-C. Shang and Y.-C. Teng (ed.) *Theoretical and computational acoustics 2005, proceedings of 7th international conference*, 2006, pp. 89-98.

[5] J.B. Pendry, *Low energy electron diffraction*, Academic Press, London, 1974.

[6] I.E. Psarobas, N. Stefanou and A. Modinos, "Scattering of elastic waves by periodic arrays of spherical bodies", *Phys. Rev. B* **62**, 278-291 (2000).

[7] Z. Liu, C.T. Shan, P. Sheng, A. L. Goertzen and J. H. Page, "Elastic wave scattering by periodic structures of spherical objects: theory and experiment", *Phys. Rev. B* **62**, 2446-2457 (2000).

[8] B.L.N. Kennett, *Seismic wave propagation in stratified media*, Cambridge Univ. Press, Cambridge, 1983.

[9] R. Sainidou, N. Stefanou, I.E. Psarobas and A. Modinos "A layer-multiple-scattering method for phononic crystals and heterostructures of such", *Comput. Phys. Commun.* **166**, 197-240 (2005).

[10] C. van Moll and D.G. Simons, "Improved performance of global optimisation methods for inversion problems in underwater acoustics", in D. G. Simons (ed.) *Proceedings of the Seventh European Conference on Underwater Acoustics*, 2004, pp. 715-720.

[11] H. Gothäll and R. Westin, "Evaluation of four global optimisation techniques (ASSA, DE, NA, Tabu Search) as applied to anechoic coating design and inverse problem uncertainty estimation", M.Sc. thesis, Swedish Defence Research Agency, 2005.

[12] M. Sambridge, "Geophysical inversion with a neighbourhood algorithm - 2 appraising the ensemble", *Geophys. J. Int.* **138**, 727-746 (1999).

[13] A. Boström "Scattering by a smooth elastic obstacle", *J. Acoust. Soc. Am.* **67**, 1904-1913 (1980).